Imaging of Advanced Neuroendocrine Tumors with ^{18}F-FDOPA PET

Alexander Becherer, MD[1,2]; Monica Szabó, MD[1]; Georgios Karanikas, MD[1]; Patrick Wunderbaldinger, MD[3]; Peter Angelberger, PhD[4]; Markus Raderer, MD[5]; Amir Kurtaran, MD[1]; Robert Dudczak, MD[1,2]; and Kurt Kletter, MD, PhD[1]

[1]Department of Nuclear Medicine, University of Vienna, Medical School, Vienna, Austria; [2]Ludwig Boltzmann Institute of Nuclear Medicine, Vienna, Austria; [3]Department of Radiology, University of Vienna, Medical School, Vienna, Austria; [4]Department of Radiopharmaceuticals, Austrian Research Centers Seibersdorf, Seibersdorf, Austria; and [5]Department of Oncology, University of Vienna, Medical School, Vienna, Austria

Nuclear medicine plays an important role in the imaging of neuroendocrine tumors (NETs). Somatostatin receptor scintigraphy (SRS) with ^{111}In-labeled somatostatin receptor analogs is a standard procedure for the detection and staging of NET. Based on the ability of NETs to store biogenic amines, this study evaluated whether 6-^{18}F-fluoro-L-DOPA (^{18}F-FDOPA) is a suitable PET tracer for NETs. **Methods:** Twenty-three patients with histologically verified NETs in advanced stages were consecutively enrolled in the study. All patients underwent PET with ^{18}F-FDOPA, CT, and SRS within 6 wk. In patients with discrepancies between nuclear medicine and radiologic methods, follow-up investigations were performed by CT, MRI, and ultrasound. ^{18}F-FDOPA PET with attenuation correction was done 30 and 90 min after injection from the neck to the upper legs. SRS was performed with ^{111}In-DOTA-D-Phe^{1}-Tyr^{3}-octreotide at 6 and 24 h. All images were read without knowledge of the results of the other modalities. In every patient, the following regions were evaluated separately: bones, mediastinum, lungs, liver, pancreas, and others, including the abdominal and supraclavicular lymph nodes, spleen, and soft- tissue lesions. The findings were confirmed by clinical examination. The nuclear medicine methods were compared against morphologic imaging, which was considered as gold standard. **Results:** The most frequently involved organs or regions were the liver (prevalence, 70%) and bone (52%), followed by mediastinal foci (31%), the lungs (22%), and the pancreas (13%). Fifty-two percent of patients had various lymphatic lesions. ^{18}F-FDOPA was most accurate in detecting skeletal lesions (sensitivity, 100%; specificity, 91%) but was insufficient in the lung (sensitivity, 20%; specificity, 94%); SRS yielded its best results in the liver (sensitivity, 75%; specificity, 100%); however, it was less accurate than PET in all organs. In about 40%, initial CT failed to detect bone metastases shown by PET that were later on verified by radiologic follow-up. **Conclusion:** ^{18}F-FDOPA PET performs better than SRS in visualizing NETs and may even do better than CT for bone lesions. SRS is essential to establish the usefulness of therapy with somatostatin analogs, yet is less accurate than ^{18}F-FDOPA PET for staging.

Received Aug. 29, 2003; revision accepted Mar. 2, 2004.

For correspondence or reprints contact: Alexander Becherer, MD, Department of Nuclear Medicine, University of Vienna, Medical School, Währinger Gürtel 18-20, A-1090 Vienna, Austria.

E-mail: alexander.becherer@meduniwien.ac.at

Key Words: neuroendocrine tumors; ^{18}F-fluorodopa; PET; somatostatin receptor scintigraphy

J Nucl Med 2004; 45:1161–1167

Neuroendocrine tumors (NETs) are a heterogeneous group of neoplasms characterized by their endocrine metabolism and histologic pattern. They have no specific primary location, yet 90% originate from the gastroenteropancreatic tract (*1*). NETs are usually of relatively low malignancy and have a slow growth rate. The primary tumor is generally small. Metastases are rarely present as long as the tumor diameter is <2 cm. Small primaries are commonly asymptomatic. The typical carcinoid syndrome with diarrhea, flush, and headache, which often leads to the diagnosis, is caused by the release of secretory products by liver metastases into the systemic circulation. Thus, many patients have metastases at the primary diagnosis. Many nonmetastasizing NETs are diagnosed incidentally.

Several imaging modalities are important in the diagnosis and staging of NETs. For small NETs of the foregut, the stomach, and the pancreas, endosonography was found to possess high sensitivity (*2*,*3*). Conventional ultrasound, CT, and MRI are used for imaging pancreatic lesions, liver lesions, and abdominal lesions. Since there is a very high expression of somatostatin receptors on NET cells, somatostatin receptor scintigraphy (SRS) has revolutionized the imaging of NETs, first with an ^{123}I label and subsequently with an ^{111}In label (*4*,*5*).

The treatment depends on the extent of tumor progression. Therefore, accurate staging is essential to establish the prognosis of the disease. Surgery is the only curative approach. SRS has become an essential feature of NET imaging, as it can assist in therapeutic decision making between surgery, embolization, or somatostatin analogs (*6*). Furthermore, there is evidence of a correlation between somatostatin receptor expression and prognosis, since SRS-positive tumors respond better to treatment with somatostatin analogs (*7*).

The ability of NETs to accumulate and decarboxylate 5′-hydroxytryptamine and L-3,4-dihydroxyphenylalanine (L-DOPA) is well known; it led to the original APUD (amine precursor uptake and decarboxylation) concept of Pearse (*8*). Increased activity of L-DOPA decarboxylase was found to be a hallmark of NETs (*9–11*). Ahlström et al. were the first to visualize pancreatic NETs with ^{11}C-labeled DOPA and PET (*12*). Based on these data and a case report (*13*), we conducted a study to determine the significance of 6-^{18}F-fluoro-L-DOPA (^{18}F-FDOPA) as a PET tracer in the imaging and staging of NETs compared with conventional SRS and CT.

MATERIALS AND METHODS

Patients

The study was designed as a phase I/phase II study to show the feasibility of NET visualization by this tracer with inclusion of patients in advanced disease stages. Twenty-three patients, 14 male and 9 female, with histologically verified metastasizing NETs were eligible for the study. Their ages at the time of investigation ranged from 42 to 81 y (mean age, 59.3 y). The primary tumors were as follows: 3 gastrinomas of the pancreas, stomach, and unknown location; 1 pancreatic glucagonoma, 1 pancreatic somatostatinoma, and 18 carcinoids, of which 4 were primarily located in the ileocecal region, a further 4 in the pancreas, 1 in the lung, 1 in the mediastinum, and 1 in the rectum. In the remaining 7 carcinoids, the primary tumor is yet to be established. Demographic data are given in Table 1. All patients had access to PET with ^{18}F-FDOPA and SRS and to CT scans within a time span of 6 wk.

PET

For the PET examination, the patients fasted for a minimum of 2 h but were well hydrated orally. ^{18}F-FDOPA (300 ± 50 MBq) was administered intravenously. After an accumulation time of approximately 30 min, which the patient spent in a supine position, an emission scan from the neck to the upper legs was performed, followed by a transmission scan. A second scan of the torso was obtained after an uptake period of 90 min. At this time, an additional scan of the brain was performed as an in vivo quality control for the radiopharmaceutical.

^{18}F-FDOPA was synthesized by an improved modification of electrophilic radiofluorination (*14*) in the radiopharmaceutical laboratory of the Austrian Research Centers Seibersdorf, Seibersdorf, Austria.

Images were taken using a full-ring PET scanner (Advance; General Electric Medical Systems) with an axial field of view of 15.2 cm. The body scans were obtained in the 2-dimensional mode, with 5-min scanning time per table position. Transmission scans with 75,000 kilocounts per table position were acquired using the built-in ^{67}Ge/^{68}Ga rod sources. Raw data were reconstructed without prefiltering, using an iterative algorithm with ordered-subset expectation maximization. Finally, the standardized uptake values (SUVs), standardized to body weight, were

TABLE 1
Patient Characteristics

Patient no.	Age (y)	Sex	Location of primary	Tumor differentiation	Tumor sites*	Therapy before PET†
1	70	M	Mediastinum	Carcinoid	b, m, lu, li	irrad, cht, oct-h
2	42	M	Pancreas	Carcinoid	p	None
3	52	F	Unknown	Carcinoid	b, o	None
4	74	F	Unknown	Carcinoid	m, li, o	surg, cht
5	67	M	Ileocecal	Carcinoid	b, li, o	surg, emb
6	72	F	Pancreas	Carcinoid	b, li	surg, irrad, cht, oct-h
7	67	F	Unknown	Carcinoid	o	surg
8	56	M	Ileocecal	Carcinoid	b, m, li, o	surg, emb, oct-c, IFN
9	45	F	Pancreas	Glucagonoma	b, li, o	surg, irrad, IFN, oct-c, oct-h
10	60	M	Pancreas	Somatostatinoma	b, li, o	surg, IFN, cht, oct-h
11	46	M	Pancreas	Carcinoid	li, p	surg, emb
12	61	M	Unknown	Carcinoid	b, m, lu, li	cht
13	45	M	Ileocecal	Carcinoid	b, li	cht, emb
14	70	M	Unknown	Carcinoid	li	surg
15	53	M	Unknown	Gastrinoma	li	surg, oct-h
16	61	F	Ileocecal	Carcinoid	m, lu, li, o	surg, emb, oct-h
17	72	F	Unknown	Carcinoid	b, m, li, o	None
18	47	F	Pancreas	Gastrinoma	li, o	surg
19	57	M	Pancreas	Carcinoid	li, p, o	cht, IFN, oct-c
20	63	F	Lung	Carcinoid	b, m, lu	surg, cht
21	69	F	Stomach	Gastrinoma	o	surg
22	81	M	Rectum	Carcinoid	b, o	irrad
23	59	M	Unknown	Carcinoid	lu, li,	surg, cht, oct-h

*Tumor sites: b = bone; m = mediastinal; lu = lung; li = liver; p = pancreatic; o = others.
†Therapies: irrad = irradiation; cht = chemotherapy; oct-h = ^{90}Y-labeled octreotide; surg = surgery; emb = embolization; oct-c = inactive octreotide; IFN = interferon-α.

calculated. Brain scans were obtained in the 3-dimensional mode, matrix size = 256 × 256 pixels, scanning time = 10 min, and reconstructed by filtered backprojection using a Hanning filter (cutoff, 6.2 mm) with elliptic attenuation correction.

SRS

After intravenous administration of 140 ± 10 MBq ^{111}In-DOTA-D-Phe^{1}-Tyr^{3}-octreotide (Austrian Research Centers Seibersdorf, Seibersdorf, Austria), planar scintigrams with a large-field-of-view, double-head, γ-camera (Millennium VG; General Electric Medical Systems) were obtained. Anterior and posterior whole-body images were obtained 4 and 24 h after injection. Images were acquired in a 256 × 256 pixel matrix in continuous acquisition mode, 5 cm/min. Additional SPECT images of the target regions were obtained after 24 h: 128 × 128 pixel matrix, 3° steps, 30 s per step, iterative reconstruction.

Morphologic Imaging

Nineteen patients underwent morphologic imaging by CT using contrast-enhanced helical CT in the Department of Radiology in our hospital; 4 patients had their CT scans at other institutions. Thoracic and abdominal CT was performed in all patients; 1 patient had an additional CT of the thighs for confirmation of a lesion with increased activity in this region that was seen in a previous PET scan. Some patients received additional ultrasound (n = 13) or MRI investigations (n = 6) during their clinical work-up. Control CT was performed 3–4 mo after the study in all patients. These CT scans were read in the soft-tissue as well as in the bone window, and particular attention was given to the presence of skeletal lesions. Further CT scans were available from the routine follow-up 6–9 mo later.

Data Analysis

The reconstructed images of the ^{18}F-FDOPA PET and the SRS were evaluated independently by 2 experienced nuclear medicine physicians, the readers were unaware of the results of the other imaging examinations. If the results were discordant, a third reader acted as referee. Any tracer accumulation exceeding the normal tissue uptake was rated as a pathologic finding. All CT images were read by a radiologist who was unaware of the results of all other imaging modalities. The images were rated positive when a focal lesion suggested a malignant appearance.

All patients had histologically verified NETs when they were included in the study. The metastatic sites were not verified by histology because of the advanced stage of disease. To verify the results of PET and SRS, CT was used as a reference. The following algorithm was used: If PET or SRS was positive in a region with clearly visible lesions on CT, the finding was considered true-positive. If all 3 were negative in a region, it was considered true-negative. If PET or SRS was negative in a region with positive CT, the findings were considered false-negative. In cases of clearly positive ^{18}F-FDOPA PET or SRS and negative CT, the latter investigation was compared with the follow-up CT scans that were obtained after 3–4 mo and after 6–9 mo. If necessary, ultrasound or MRI was additionally performed. When the morphologic findings remained unequivocally negative, the nuclear medicine findings were rated as false-positive; when the radiologic imaging turned positive in the region in question, nuclear medicine imaging was considered true-positive.

A lesion-by-lesion comparison for the calculation of sensitivity and specificity was not performed because some patients had numerous lesions, which rendered a lesion-based assessment inaccurate. Instead, we determined an organ-based sensitivity and specificity. The following 6 organ systems were assessed separately: skeleton, mediastinum, lungs, liver, pancreas, and lymph nodes. The organs were rated positive if there were abnormal hot spots or focal abnormalities, regardless of their numbers. The 95% confidence intervals were calculated by binomial expansion.

RESULTS

A total of 138 regions were evaluated; 57 regions had pathologic findings. Detailed data concerning the organ-based sensitivities and specificities are given in Table 1. CT scans showed diffuse metastasis to the liver, which resulted in numerous lesions in 3 patients (Fig. 1; patients 9, 10, and 12). In one of these patients, the same was true for the lungs (patient 12). ^{18}F-FDOPA PET failed to show the lung lesions and the liver lesions in the latter patient, whereas SRS was able to show 1 liver lesion. In the remaining 2 patients, PET visualized 7 and 2 liver lesions, whereas SRS showed 4 and 5 lesions, respectively. Visualization of the gallbladder and the pancreas was a frequent, yet inconstant, finding. Gallbladder activity could be recognized well and caused no problems in scan interpretation. Pancreatic activity was considered normal if it was of diffuse nature.

^{18}F-FDOPA PET was most sensitive in visualizing skeletal lesions and mediastinal lesions with a sensitivity of 100% (Fig. 2). It also showed all pancreatic lesions in the 3 patients with involvement of the pancreas. The sensitivity of PET was lowest in the lungs, where it showed only 1 of 5 affected lungs (sensitivity, 20%). The undetected lesions were of small size. Most of them were <5 mm; the largest had a maximal diameter of 8 mm. The specificity of PET was 81.3% for the liver, 90.9% for the skeleton, and 100% for the mediastinum, the pancreas, and lymph nodes.

SRS showed the highest sensitivity (81.8%) for lymph nodes, followed by the liver (75.0%), whereas it was unable to show any lung lesion. The specificity of SRS was 94.4% in the lungs and 100% in all other organs.

The results of CT that was performed parallel to ^{18}F-FDOPA PET and SRS and the final results based on the subsequent follow-up morphologic imaging are given in Table 2. Table 3 shows the diagnostic performance of ^{18}F-FDOPA PET and SRS. Sensitivity and specificity for ^{18}F-FDOPA PET and SRS were calculated using the final results of morphologic imaging.

The visual interpretation revealed no advantage of the 90-min scan over the 30-min scan. The lesion SUVs ranged from 1.6 to 15.0 at 30 min after injection and from 1.5 to 17.1 at 90 min after injection, with no statistically significant difference.

DISCUSSION

Because of the enhanced expression of somatostatin receptors, most NETs are visualized by functional imaging with the ^{111}In-labeled somatostatin analog pentetreotide (*5*,*15*). By identifying previously undetected metastases,

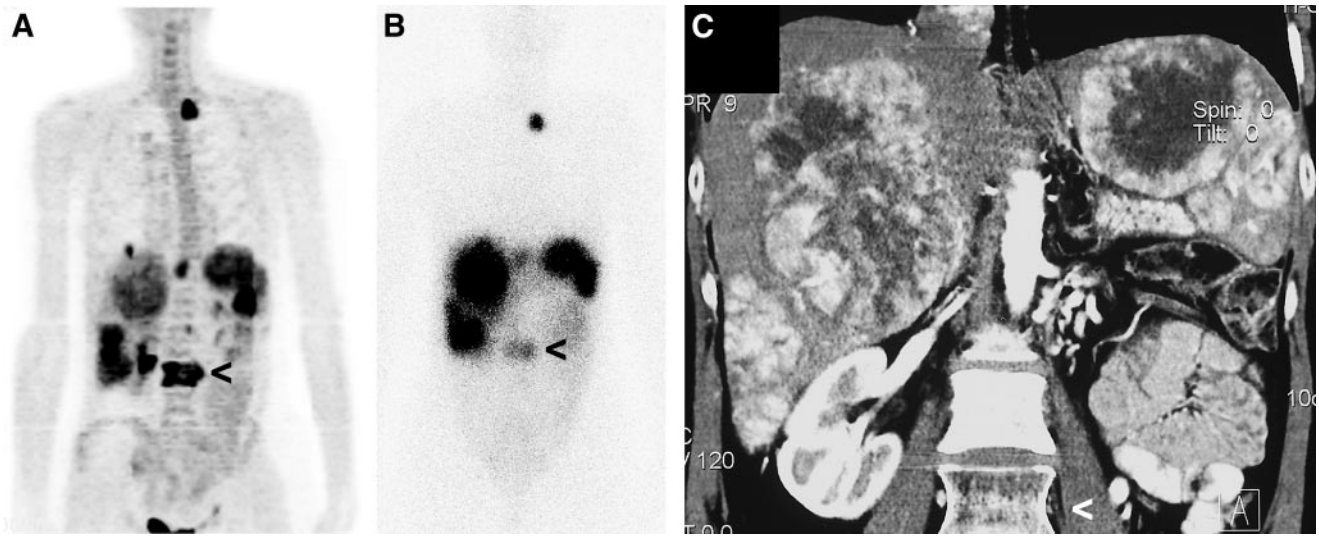

FIGURE 1. ^{18}F-FDOPA PET (A), SRS (B), and multislice CT (C) in patient with metastasizing glucagonoma of pancreas. Note extensive liver metastasis with massive enlargement of both liver lobes, particularly the left lobe (patient had splenectomy); lymph node metastasis in left supraclavicular region and in epigastrium; and bone metastasis in lumbar spine. Also note better resolution of PET images compared with SRS. Involved lumbar vertebra is clearly shown by ^{18}F-FDOPA PET but has only weak uptake in SRS (arrowhead). CT could not differentiate between vital tumor in lumbar spine and changes after irradiation.

SRS may instigate a change of management in up to a third of patients (*16*). However, the spatial resolution of SRS is markedly poorer than that of CT or MRI; thus, an exact topographic description of pathologic findings is rendered difficult. PET, which was shown to be very useful in a variety of malignancies, is able to partly overcome this difficulty. The widely used ^{18}F-FDG is of limited value in NETs because these tumors usually do not show enhanced FDG uptake (*17*). PET, however, offers the opportunity to design tracers chemically close or identical to pathophysiologic substrates, which is of great interest in NETs. PET scans with ^{11}C-labeled 5-hydroxytryptophan and ^{11}C-DOPA were able to visualize these tumors (*12*,*18*).

Encouraged by a case report of Hoegerle et al., we compared ^{18}F-FDOPA PET and SRS with CT in terms of imaging accuracy in patients with known NETs (*13*). With respect of overall diagnostic performance, ^{18}F-FDOPA PET and SRS had a high specificity of nearly 100%. The sensitivity of ^{18}F-FDOPA PET was approximately 85%, whereas that of SRS was markedly lower—that is, 58%. A similar observation was made in a recently published study that also compared SRS, ^{18}F-FDOPA PET, and morphologic imaging (*19*). However, this recent study differed from the present study in the following respects: The lesions were categorized as primaries, lymph nodes, and organ metastases, but no further information about the location was given. A further difference is that 6 of 17 patients underwent abdominal morphologic imaging only by MRI and not by CT; however, all patients underwent thoracic CT. Finally, Hoegerle et al. achieved a consensus for the final rating of a tumor as positive or negative on the basis of the total number of lesions. This might account for the 20% lower sensitivity of ^{18}F-FDOPA PET of 65% established by Hoegerle. We calculated the sensitivities based on the involvement of body regions, not on the number of lesions, because of the large number of lesions in several patients. Furthermore, in advanced tumors with multiple organ involvement, the clinical consequence of numerous lesions in one and the same organ is uncertain. Hoegerle et al. scanned at 60 min after injection. We compared scans at 30 min with scans at 90 min and found no differences either visually or in the SUVs. Thus, for logistic lesions, a scan starting 30–45 min after injection should be sufficient. To the best of our knowledge, this study and ours are the only 2 systematic investigations of NET imaging with ^{18}F-FDOPA PET. Hoegerle et al. were also able to show the usefulness of ^{18}F-FDOPA PET in medullary thyroid carcinoma and pheochromocytoma (*20*,*21*). Further studies will hopefully provide more insight into the diagnostic abilities of this tracer in NETs and on the uptake mechanisms.

Subdividing our results into organs and regions, SRS and ^{18}F-FDOPA PET yielded different sensitivities. ^{18}F-FDOPA PET was able to show skeletal involvement markedly better than SRS (sensitivity, 100% vs. 50%). CT showed bony involvement less accurately than ^{18}F-FDOPA PET. This finding is in accordance with the study of Chiti et al., who compared SRS with CT and ultrasound as diagnostic tools for NETs. The authors concluded that these imaging modalities are not the procedures of choice for visualization of skeletal metastases (*22*).

In the lungs, ^{18}F-FDOPA PET and SRS were unsatisfactory (sensitivity, 20% vs. 0%) whereas, with respect to mediastinal lymph node involvement, PET and CT seem to be comparable. In lung imaging, PET may suffer from respiratory excursions of the thorax, whereas CT is acquired during breath hold. The movement of the mediastinum,

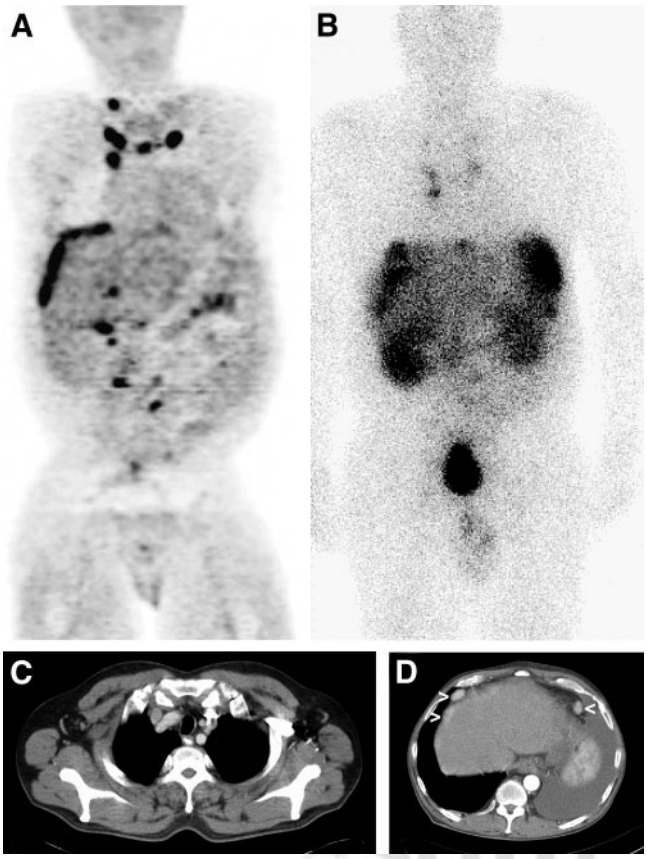

FIGURE 2. (A) Visualization of multiple rib lesions and one sternal lesion by ^{18}F-FDOPA PET in addition to carcinosis in liver capsule and multiple abdominal nodes of ileocecal carcinoid. (B) SRS shows rib lesions less clearly and misses sternal lesion and some of abdominal nodes. (C) CT of thorax failed to reveal any of the bone lesions. (D) Abdominal CT shows subcapsular liver metastases and lymph node metastases (arrowheads). Note obvious contrast-enhancing liver capsule indicative of diffuse infiltrative metastatic tumor spread. Left-sided pleural effusion is evident (D).

however, is negligible, which could at least partially account for the difference in sensitivity compared with that in the lungs. Pulmonary disease is not common. Primary carcinoids of the lungs account for no more than 10% of all NETs, whereas pulmonary metastasis is present in about 10% (*1*).

The liver is the main location of gastroenteropancreatic NET metastasis, being affected in 42%–95% of cases (*23,24*). We found liver metastases in 17 of 23 patients (74%), which is in good agreement with the study of Nocaudie-Calzada et al., where hepatic invasion was present in 21 of 31 patients (68%) (*25*). In liver lesions, these authors established a sensitivity of 80% for SRS but a sensitivity of 100% for morphologic imaging. In our study, the sensitivity of SRS in the liver was 75%, whereas that of ^{18}F-FDOPA PET was 81.3%. CT showed pathologic liver findings in 15 of 16 patients in whom liver lesions were eventually detected. The specificity of PET was 85.7% versus 100% of SRS due to a false-positive PET finding in a lesion after embolization.

In all other regions, especially in abdominal nodes and intestinal tumors, ^{18}F-FDOPA PET and CT were similar. PET had a sensitivity of 92.3%, which was superior to SRS, with a sensitivity of 76.9%. It has been reported that, in NET, metastases might not be shown by SRS, probably due to a different receptor pattern (*26,27*). Why some lesions were not seen on ^{18}F-FDOPA PET is unclear at this time. One possible explanation might be found in the different behavior of some lesions and whole tumors with regard to the expression of DOPA decarboxylase, analogous to the heterogeneity of receptor expression.

Accurate staging in NETs is important not only for defining suitable candidates for surgery but also for prognostic reasons. Reed proposes a categorization of patients into 6 subtypes, based on the aggressiveness of disease management after initial therapy (*16*):

0. Complete excision with normal scan and markers.
1. Asymptomatic “small volume” disease.
2. Symptomatic “large volume” disease.
3. Symptomatic with good performance status.
4. Symptomatic with poor performance status.
5. Anaplastic or undifferentiated tumors.

The higher diagnostic accuracy of ^{18}F-FDOPA PET compared with SRS might help to optimize treatment. Groups 0 and 1, which only need regular follow-up, might be confirmed more reliably by ^{18}F-FDOPA PET. On the other hand, in categories 2 and 3, a sensitive modality for tumor search is absolutely essential to define sites of tumor progression, in particular when local complications are likely to occur—for example, obstruction in intestinal tumors or fractures in bone tumors. Particularly in NETs of the small bowel, which have the highest risk of metastasis—mainly into the liver—a sensitive whole-body scanning method is beneficial (*28*).

It has to be noted that the nuclear medicine modalities reflected only one point in time while the gold standard by morphologic imaging consisted of the initial CT and follow-up investigations. Looking solely at the initial CT that was performed within 6 wk of ^{18}F-FDOPA PET and SRS, several negative CT findings occurred, which turned out to

TABLE 2
Involved Organs with Diagnosis by Initial CT in Comparison with Follow-Up Results

Organ	Initial CT	Final result
Bone	8	12
Mediastinum	6	7
Lungs	5	5
Liver	15	16
Pancreas	2	3
Lymph nodes	12	11

TABLE 3
Sensitivity and Specificity of SRS and PET in Different Organs and Regions

Parameter	Bone		Mediastinum		Lungs		Liver		Pancreas		Lymph nodes	
	SRS	PET	SRS	PET	SRS	PET	SRS	PET	SRS	PET	SRS	PET
True-negative	11	10	16	16	17	17	7	6	20	20	12	12
True-positive	6	12	3	7	0	1	12	13	2	3	9	10
False-negative	6	0	4	0	5	4	4	3	1	0	2	1
False-positive	0	1	0	0	1	1	0	1	0	0	0	0
Prevalence	52.2		30.3		21.7		69.7		13.0		47.8	
Sensitivity (%)	50.0	100.0	42.9	100.0	0.0	20.0	75.0	81.3	66.7	100.0	81.8	90.9
	(21–87)	(73–100)	(9–85)	(59–100)	(0–87)	(0–89)	(47–93)	(54–98)	(9–91)	(29–100)	(48–95)	(58–97)
Specificity (%)	100.0	90.9	100.0	100.0	94.4	94.4	100.0	85.7	100.0	100.0	100.0	100.0
	(71–100)	(56–99)	(79–100)	(79–100)	(72–99)	(72–99)	(59–100)	(42–99)	(83–100)	(83–100)	(73–100)	(73–100)
PPV	100.0	92.3	100.0	100.0	0.0	50.0	100.0	92.9	100.0	100.0	100.0	100.0
	(54–100)	(63–99)	(29–100)	(59–100)	(0–99)	(1–99)	(73–100)	(66–99)	(15–100)	(29–100)	(66–100)	(69–100)
NPV	64.7	100.0	80.0	100.0	77.3	81.0	63.7	66.7	95.2	100.0	85.7	90.9
	(38–85)	(69–100)	(56–94)	(79–100)	(54–92)	(58–94)	(30–89)	(29–92)	(47–99)	(83–100)	(51–97)	(63–99)

PPV = positive predictive value; NPV = negative predictive value.
95% confidence intervals are in parentheses.

be false-negative, in particular in the skeleton. ^{18}F-FDOPA PET displayed, by >40%, more skeletal lesions than CT.

The study did not aim to assess the influence of the method on therapeutic strategies. Hoegerle et al., however, demonstrated that ^{18}F-FDOPA PET could alter patient management in 30% of the cases (*19*). The advanced tumor stages of our patients were probably the most important reason why ^{18}F-FDOPA PET did not influence further treatment; in the presence of a high tumor load, the range of therapeutic options is limited.

Because it was not possible to obtain histologic verification of the findings, follow-up by morphologic imaging had to be used as the gold standard. This might be somewhat problematic because lesions not seen by nuclear medicine imaging or by CT remain undetected. Nevertheless, such lesions probably would escape early noninvasive diagnosis even otherwise. In turn, some lesions displayed on ^{18}F-FDOPA PET and SRS but not on CT, and thus finally classified as false-positive, might have escaped detection even by follow-up radiology. Especially in bone lesions, ^{18}F-FDOPA PET demonstrated lesions that were eventually shown on later radiologic imaging. Perhaps some of the false-positive lesions were not yet proven by follow-up but had been found in later investigations.

CONCLUSION

CT offers the highest diagnostic potential for assessment of lung and liver involvement in patients with a NET. SRS is readily available and assists in decisions about treatment with somatostatin analogs, either unlabeled or radiolabeled. Therefore, SRS still is an important radionuclide imaging method in NETs. ^{18}F-FDOPA PET, however, is more accurate than conventional radionuclide imaging using SRS, as it is markedly superior to the latter in detecting bone metastases and might even be better than CT in this respect. We consider ^{18}F-FDOPA PET a promising staging modality. Larger patient numbers will clarify the clinical value of this new method.

ACKNOWLEDGMENTS

We thank Sujata Wagner for reviewing the manuscript. This study was supported by grant 1863/00 of the Lord Mayor of Vienna (Bürgermeisterfonds). Part of this study was presented at the 50th Annual Meeting of the Society of Nuclear Medicine, New Orleans, LA, June 21–25, 2003.

REFERENCES

1. Caplin ME, Buscombe JR, Hilson AJ, Jones AL, Watkinson AF, Burroughs AK. Carcinoid tumour. *Lancet.* 1998;352:799–805.
2. Zimmer T, Ziegler K, Liehr RM, Stolzel U, Riecken EO, Wiedenmann B. Endosonography of neuroendocrine tumors of the stomach, duodenum, and pancreas. *Ann NY Acad Sci.* 1994;733:425–436.
3. De Angelis C, Carucci P, Repici A, Rizzetto M. Endosonography in decision making and management of gastrointestinal endocrine tumors. *Eur J Ultrasound.* 1999;10:139–150.
4. Kwekkeboom DJ, Krenning EP, Bakker WH, et al. Radioiodinated somatostatin analog scintigraphy in small-cell lung cancer. *J Nucl Med.* 1991;32:1845–1848.
5. Krenning EP, Kwekkeboom DJ, Reubi JC, et al. ^{111}In-Octreotide scintigraphy in oncology. *Metabolism.* 1992;41:83–86.
6. Slooter GD, Mearadji A, Breeman WA, et al. Somatostatin receptor imaging, therapy and new strategies in patients with neuroendocrine tumours. *Br J Surg.* 2001;88:31–40.
7. Kvols LK, Reubi JC, Horisberger U, Moertel CG, Rubin J, Charboneau JW. The presence of somatostatin receptors in malignant neuroendocrine tumor tissue predicts responsiveness to octreotide. *Yale J Biol Med.* 1992;65:505–518.
8. Pearse AG. The cytochemistry and ultrastructure of polypeptide hormone-producing cells of the APUD series and the embryologic, physiologic and pathologic implications of the concept. *J Histochem Cytochem.* 1969;17:303–313.
9. Baylin SB, Abeloff MD, Goodwin G, Carney DN, Gazdar AF. Activities of L-dopa decarboxylase and diamine oxidase (histaminase) in human lung cancers and decarboxylase as a marker for small (oat) cell cancer in cell culture. *Cancer Res.* 1980;40:1990–1994.
10. Berger CL, de Bustros A, Roos BA, et al. Human medullary thyroid carcinoma

in culture provides a model relating growth dynamics, endocrine cell differentiation, and tumor progression. *J Clin Endocrinol Metab.* 1984;59:338–343.
11. Gazdar AF, Helman LJ, Israel MA, et al. Expression of neuroendocrine cell markers L-dopa decarboxylase, chromogranin A, and dense core granules in human tumors of endocrine and nonendocrine origin. *Cancer Res.* 1988;48: 4078–4082.
12. Ahlström H, Eriksson B, Bergstrom M, Bjurling P, Langstrom B, Oberg K. Pancreatic neuroendocrine tumors: diagnosis with PET. *Radiology.* 1995;195: 333–337.
13. Hoegerle S, Schneider B, Kraft A, Moser E, Nitzsche EU. Imaging of a metastatic gastrointestinal carcinoid by F-18-DOPA positron emission tomography. *Nuklearmedizin.* 1999;38:127–130.
14. Fuchtner F, Angelberger P, Kvaternik H, Hammerschmidt F, Simovc BP, Steinbach J. Aspects of 6-[^{18}F]fluoro-L-DOPA preparation: precursor synthesis, preparative HPLC purification and determination of radiochemical purity. *Nucl Med Biol.* 2002;29:477–481.
15. Kwekkeboom DJ, Krenning EP. Somatostatin receptor scintigraphy in patients with carcinoid tumors. *World J Surg.* 1996;20:157–161.
16. Reed NS. Management of neuroendocrine tumours. *Clin Oncol* (*R Coll Radiol*). 1999;11:295–302.
17. Eriksson B, Bergstrom M, Orlefors H, Sundin A, Oberg K, Langstrom B. Use of PET in neuroendocrine tumors: in vivo applications and in vitro studies. *Q J Nucl Med.* 2000;44:68–76.
18. Eriksson B, Bergstrom M, Lilja A, Ahlstrom H, Langstrom B, Oberg K. Positron emission tomography (PET) in neuroendocrine gastrointestinal tumors. *Acta Oncol.* 1993;32:189–196.
19. Hoegerle S, Altehoefer C, Ghanem N, et al. Whole-body ^{18}F dopa PET for detection of gastrointestinal carcinoid tumors. *Radiology.* 2001;220:373–380.
20. Hoegerle S, Altehoefer C, Ghanem N, Brink I, Moser E, Nitzsche E. ^{18}F-DOPA positron emission tomography for tumour detection in patients with medullary thyroid carcinoma and elevated calcitonin levels. *Eur J Nucl Med.* 2001;28: 64–71.
21. Hoegerle S, Nitzsche E, Altehoefer C, et al. Pheochromocytomas: detection with ^{18}F DOPA whole body PET—initial results. *Radiology.* 2002;222:507–512.
22. Chiti A, Fanti S, Savelli G, et al. Comparison of somatostatin receptor imaging, computed tomography and ultrasound in the clinical management of neuroendocrine gastro-entero-pancreatic tumours. *Eur J Nucl Med.* 1998;25: 1396–1403.
23. Raderer M, Kurtaran A, Leimer M, et al. Value of peptide receptor scintigraphy using ^{123}I-vasoactive intestinal peptide and ^{111}In-DTPA-D-Phe^{1}-octreotide in 194 carcinoid patients: Vienna University Experience, 1993 to 1998. *J Clin Oncol.* 2000;18:1331–1336.
24. Orlefors H, Sundin A, Ahlstrom H, et al. Positron emission tomography with 5-hydroxytryprophan in neuroendocrine tumors. *J Clin Oncol.* 1998;16:2534–2541.
25. Nocaudie-Calzada M, Huglo D, Carnaille B, Proye C, Marchandise X. Comparison of somatostatin analogue and metaiodobenzylguanidine scintigraphy for the detection of carcinoid tumours. *Eur J Nucl Med.* 1996;23:1448–1454.
26. Le Rest C, Bomanji JB, Costa DC, Townsend CE, Visvikis D, Ell PJ. Functional imaging of malignant paragangliomas and carcinoid tumours. *Eur J Nucl Med.* 2001;28:478–482.
27. Gabriel M, Decristoforo C, Donnemiller E, et al. An intrapatient comparison of ^{99m}Tc-EDDA/HYNIC-TOC with ^{111}In-DTPA-octreotide for diagnosis of somatostatin receptor-expressing tumors. *J Nucl Med.* 2003;44:708–716.
28. Sjoblom SM. Clinical presentation and prognosis of gastrointestinal carcinoid tumours. *Scand J Gastroenterol.* 1988;23:779–787.